Low-Temperature, Single-Source, Chemical Vapor Deposition of Molybdenum Nitride Thin Films

Michael A. Land,[*a] *Justin T. Lomax,*[b] *and Seán T. Barry.*[a]

[a] Department of Chemistry, Carleton University, Ottawa, Ontario K1S 5B6 Canada

[b] Department of Chemistry, University of Western Ontario, London, Ontario N6A 3K7, Canada

Keywords: Molybdenum Nitride, Single-Source, Chemical Vapor Deposition, Thin Films, Molybdenum Imides, Decomposition

Abstract

The 1,4-di-*tert*-butyl-1,3-diazabutadiene adduct of bis(*tert*-butylimido)dichloro-molybdenum(VI), (^{t}BuN)$_2$MoCl$_2$·dad, was used as a single-source precursor for the chemical vapor deposition of molybdenum nitride from 350 – 600ºC. Deposition at 400 ºC had a growth rate of 55 nm·h^{-1} and was comprised of a mixture of Mo_2N and MoN, based on X-ray photoelectron spectroscopy and grazing-incidence X-ray diffraction results. The films are essentially featureless and are as smooth as the underlying substrate, based on atomic force microscopy measurements. Because the depositions could be carried out at a low temperature there was minimal carbon (1.4%) inclusion in the film as shown by XPS.

Introduction

Molybdenum nitride thin films have a wide range of industrially relevant applications, which include microelectronic manufacturing,[1,2] hard protective coatings,[3–5]

batteries,[6,7] high surface area heterogeneous catalysis,[8] as well as super conducting materials.[9,10] One common method used to prepare Mo-containing thin films with sub-nanometer thickness control is chemical vapor deposition (CVD). Metal organic CVD relies on chemical precursors that can be delivered in the vapor phase to the substrate, which subsequently undergoes gas-surface reactions to produce thin target films.

A common class of volatile molybdenum-containing precursors are bis(*tert*-butylimido)-molybdenum(VI) compounds. For example, bis(*tert*-butylimido)-bis(dimethylamido)molybdenum(VI) (**A**) (Chart 1),[11,12] has been used to prepare MoC_xN_y films using H_2 plasma; these were found to have nearly equivalent Mo, C, and N stoichiometry.[13] Compound **A** has also been used a single-source precursor (SSP) at 450 ºC to prepare MoC_xN_y films, with *ca.* 20% carbon incorporation.[11] The structurally similar amido complex **B** has also been used for the single-source CVD of MoC_xN_y films with carbon incorporation ranging from 12% to 33%, in correspondence with an increase in the deposition temperature from 500 ºC to 650 ºC.[14] Simple structural modifications to this general framework have also been performed by changing the heteroatom of the anionic ligand, to yield, for example, the thiolate **C**.[2,15] This compound has been used as a SSP for the aerosol-assisted CVD of nitrogen-doped MoS_2 between 400 ºC and 550 ºC, however the compositional change with respect to temperature was not reported.[15]

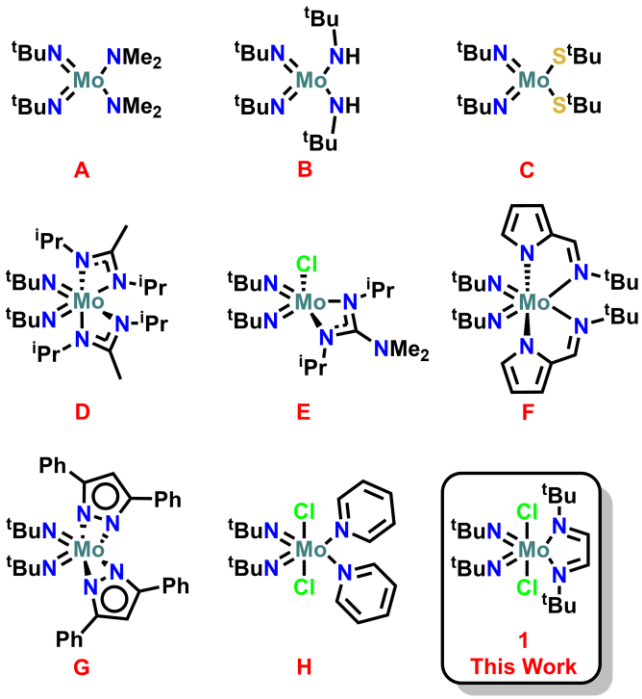

Chart 1: MoN_x and MoC_xN_y CVD precursors that contain the bis(*tert*-butylimido)molybdenum(VI) framework.

To further functionalize and explore ligand effects on the general bis(*tert*-butylimido)-molybdenum(VI) framework, complexes incorporating chelating ligands, such as *N,N'*-diisopropyl-acetamidinate, have been prepared.[16,17] The amidinate-containing compound **D** has been used as a single-source CVD precursor, however, it preferentially forms MoC_x films between 500 ºC and 800 ºC.[18] In contrast, when the CVD using **D** as a precursor is performed in the presence of NH_3 as a co-reagent, MoN_x films are obtained without carbon incorporation, but at elevated temperatures.[16,18] A structurally similar chelating ligand, *N,N*-dimethyl-*N*',*N*''-diisopropylguanidinate, has been used to prepare **E**. Only one equivalent of the chelating ligand was incorporated into the product due to increased steric demands of this ligand.[17] CVD experiments using **E** and H_2 as a reactive gas between 500 ºC and 800 ºC resulted in the formation of Mo_2C films with <5% nitrogen

incorporation.[19] When CVD experiments using **E** as a precursor and NH_3 as a co-reactant were performed Mo_2N films were obtained with *ca*. 9% carbon incorporation.[19]

We have recently reported the use of another chelating ligand, *N*-2-(tert-butyliminomethyl)pyrrolate, to prepare **F**, a compound which exhibits excellent thermal stability, forming a stable surface species until at least 500 ºC.[20] Preliminary experiments using **F** as a single-source CVD precursor at 600 ºC resulted in a MoC_xN_y film.[20] Finally, a chelating pyrazole ligand has been incorporated into the bis(*tert*-butylimido)-molybdenum(VI) framework, to yield **G**.[21] Thermolysis of **G** at 800 ºC, in the absence of a co-reagent, resulted in the formation of Mo_2N nanoparticles which were embedded in an amorphous carbon-oxygen matrix. Bulk analysis revealed a 64% carbon composition, suggesting that if **G** was to be used as a single-source CVD precursor the resulting films would also have a large carbon composition.[21]

Nitrogen incorporation into these films is a result of *γ*-H transfer of the *tert*-butylimido ligands,[14–16,20–22] leading to isobutylene elimination, which we have described in detail previously.[23] The presence of carbon likely results from the *β*-CH_3 activation of the same ligands, leading to the formation of a Mo−CH_3 species, after acetonitrile elimination.[14,22] These methyl groups can then either react with a proton source, resulting in the generation of CH_4 or undergo further C−H activation to form the carbidic atoms in the film.[14,24] The *β*-CH_3 decomposition route likely has a higher activation barrier,[14,24–26] thus explaining the increased carbon content observed in the films deposited with higher temperatures. Additionally, the CH_4 that forms as a by-product of *β*-CH_3 activation can react with a growing MoN_x film, converting it to MoC_x, a process which has previously

been shown to occur above 400 ºC (Equation 1).[27] This provides a possible explanation why the films prepared from the single-source CVD of **D** and **E** did not contain nitrogen.

$$2\ Mo_2N + 2\ CH_4 \rightarrow\ 2\ Mo_2C + 4\ H_2 + N_2 \qquad (1)$$

All of the compounds described above (Chart 1) are prepared in a two-step process from the 1,2-dimethoxyethane adduct of $(^tBuN)_2MoCl_2$, with the chloride ligands subsequently replaced by other anionic ligands. The imide ligands are the source of nitrogen in many of the films described herein, suggesting that adducts of $(^tBuN)_2MoCl_2$ itself should also make suitable precursors for the CVD of MoN_x. However, the higher temperatures required to achieve single-source CVD enables high energy decomposition pathways, including those that can lead to carbon incorporation.[14] Additionally, simple neutral ligand exchange reactions often require shorter reaction times, give higher yields, and allow easier purification compared to anionic ligand exchange reactions. Thus, we decided to explore the use of $(^tBuN)_2MoCl_2$ compounds incorporating neutral ligands as precursors for the low temperature CVD of MoN_x.[28,29] The bis-pyridine compound **H** has previously been used as a precursor for the CVD of MoC_xN_y, in the presence of H_2,[22] however, we recently showed that **H** loses one of its pyridine ligands upon heating,[28] which would lead to inconsistent gas-phase precursor composition. Therefore, we decided to explore $(^tBuN)_2MoCl_2$·dad (dad = 1,4-di-tert-butyl-1,3-diazabutadiene) (**1**) as a precursor for single-source CVD of MoN_x: it was the most volatile $(^tBuN)_2MoCl_2$ adduct among those previously reported,[29] and we knew that its neutral ligand would remain coordinated to the metal center during volatilization.[23]

Results and Discussion

Precursor Assessment and Reactivity

We have previously shown that **1** is both volatile and sufficiently thermally stable,[23,29] but to further determine if it would be a suitable deposition precursor, it was held in a stainless-steel bubbler and heated to 110 ºC for 2 hours under static vacuum. After cooling to room temperature, this process was repeated three more times to test the long-term thermal behaviour in process-like conditions. Characterization by ^{1}H NMR spectroscopy after repeated heating/cooling showed no signs of decomposition, suggesting that **1** would be thermally stable in the precursor bubbler on the timescale of a deposition experiment. We then placed **1** in a Schlenk tube and thoroughly heated it with a propane torch, causing the entirety of the Schlenk tube to be coated in a mirror-like metallic film (Figure 1). A glass substrate that had also been placed in the Schlenk flask was analyzed by energy dispersive X-ray spectroscopy (EDS) revealing a molybdenum-containing coating. These combined results were sufficient evidence to justify the further exploration of **1** as a CVD precursor.

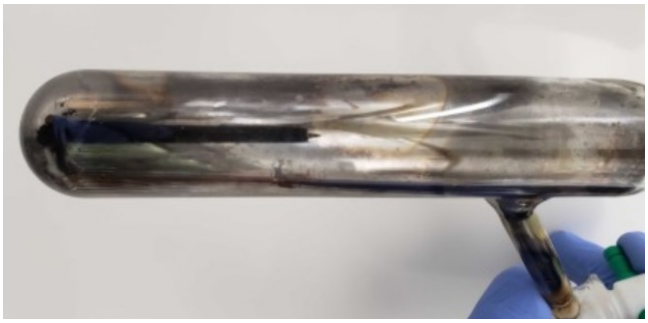

Figure 1: Photograph of a molybdenum-containing film obtained from the thermolysis of **1** inside a Schlenk tube.

Chemical Vapor Deposition and Surface Morphology

Initial optimization of precursor delivery was performed using a quartz crystal microbalance (QCM). The optimal evaporation temperature of **1** was determined to be 105 ºC, using 50 sccm of N_2 as a carrier gas. Using these conditions, continuous growth was observed by QCM beginning at 350 ºC, suggesting that this was the onset

temperature for CVD-type growth (Figure S1). After optimizing the initial parameters, **1** was delivered into a home-built, horizontal flow, low-pressure, hot-walled CVD/ALD instrument (see experimental for details) and lustrous thin films were grown on soda lime glass microscope slides between 350 ºC and 600 ºC (Figure 2b); experiments performed at 300 ºC and 325 ºC did not produce films. Each deposition was conducted over 2 hours, and the film thicknesses were measured using their cross-sections with a scanning electron microscope (SEM, Figure 2c). The resulting Arrhenius plot, showing the dependency of film growth rates on deposition temperature, had three growth regimes (Figure 2a). The kinetically limited growth regime occurred below 400 ºC and exhibited growth rates of 18-55 $nm \cdot h^{-1}$. The activation barrier for film growth in this regime was 79 ± 14 $kJ \cdot mol^{-1}$, equivalent to that reported for the CVD of WN_x using $(^tBuN)_2W(HN^tBu)_2$ as a SSP.[30] The mass transport region (450-550 ºC) intersected the kinetically limited growth regime at 407 ºC with a growth rate of 71-77 $nm \cdot h^{-1}$. In comparison, the bis-pyridine adduct **H** had a reported growth rate of 60 $nm \cdot h^{-1}$ at 450 ºC, using H_2 as a reactive gas. The deposition performed at 600 ºC showed a significant reduction in film thickness, with a growth rate of 45 $nm \cdot h^{-1}$, possibly as a result of gas-phase decomposition of the precursor before it could undergo chemisorption at the surface.

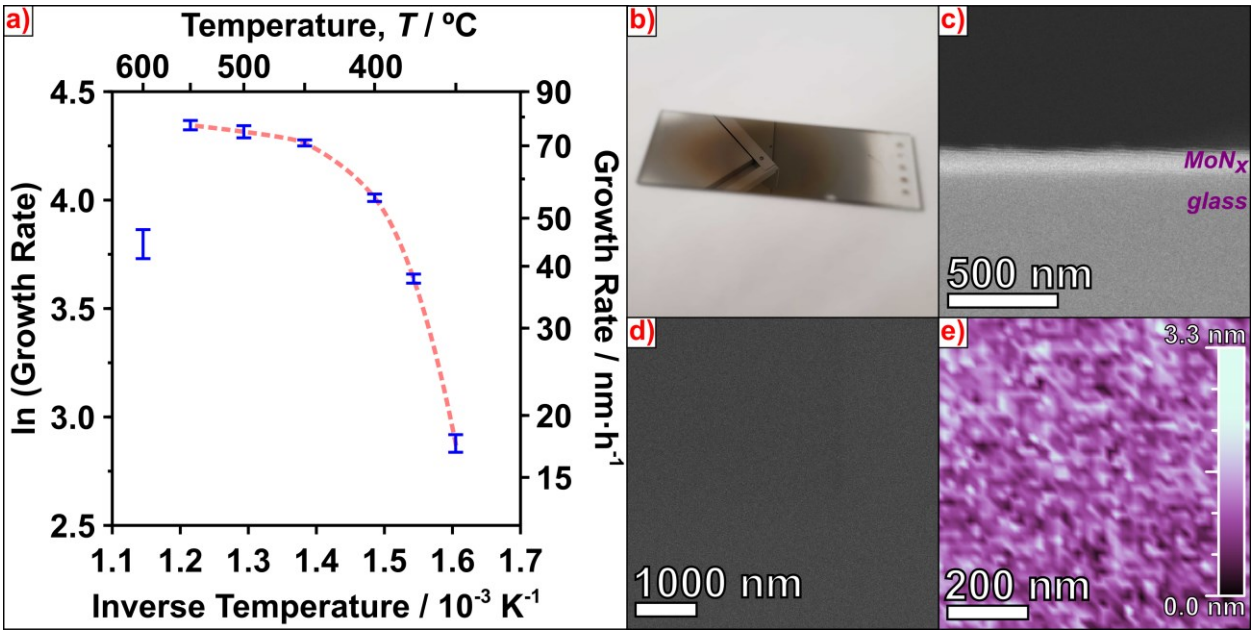

Figure 2: (a) Arrhenius plot for MoN_x thin films grown on soda lime glass substrates by CVD using **1** as a SSP; film thicknesses were measured using cross-sectional SEM. (b)

Reflective MoN_x film deposited on soda lime glass over 2 h at 400 ºC. (c) Cross-sectional SEM image, (d) plane-view SEM image, and (e) AFM image, of the same film in Figure 2b.

The lustrous films deposited above 400 ºC on soda lime glass consistently had small regions of cracking or delamination. Notably, this was not an effect of degradation of the soda lime glass, as we had previously deposited similar films at 600 ºC without these observations.[20] The films deposited at 400 ºC did not show signs of cracking, and were well adhered to the substrate, passing a “Scotch tape” test. Additionally, these films were conformal and had a high growth rate, making them suitable candidates for more thorough investigation and characterization.

Aside from the macroscale cracking/delamination just mentioned, all of the films appeared smooth and featureless by plane-view SEM (Figure 2d), and film smoothness was further verified using cross-sectional SEM. Atomic force microscopy of a 110 nm film deposited at 400 ºC revealed a root-mean-square roughness (R_{rms}) of 5.0 (± 0.2) Å (Figure 2e), which was equivalent to that measured for the untreated glass substrate (5.1 (± 0.1) Å). Attempts to perform AFM on the films deposited above 400 ºC were unsuccessful because the AFM tip delaminated the films from the substrate. To the best of our knowledge, the surface roughness of MoN_x films prepared by single-source CVD have not been previously reported. The closest example found reports a R_{rms} of 11 Å for a 25 nm thick $MoC_{0.5}N_{0.3}$ film deposited by CVD using $Mo(CO)_6$ and NH_3 at 150 ºC.[9] The lack of roughness data in the literature possibly results from most CVD MoN_x films being crystalline. In contrast, the films reported here are smooth and possibly amorphous (*vide infra*).

An overlooked aspect of CVD is the effect of deposition time on film growth, which is often also coupled with the assumption of a constant growth rate throughout the course of a deposition experiment. Using the optimized deposition parameters, thin films were deposited at 400 ºC, using times between 15 min and 5 h (Figure 3a). The resultant films changed from dull black to mirror-like in appearance with increasing deposition time, and all the films showed transmittance of visible light up until 110 nm (Figure S7). Analysis of the growth rate revealed two different growth regimes. Initially, the CVD process at 400

ºC had a growth rate of 89 nm·h^{-1}. When the film reached a thickness of 75 nm (determined by the intersection of the two regimes, Figure 3a), the growth rate decreased to 35 nm·h^{-1}. These thickness measurements were determined using both cross-sectional SEM and AFM step edge measurements, and they were also reproduced using Si(100) substrates (Figures S4 and S6). Preliminary experiments also showed the potential for film deposition on other substrates (Au, Cu, Ni, Al_2O_2), however this was not further explored in the present study.

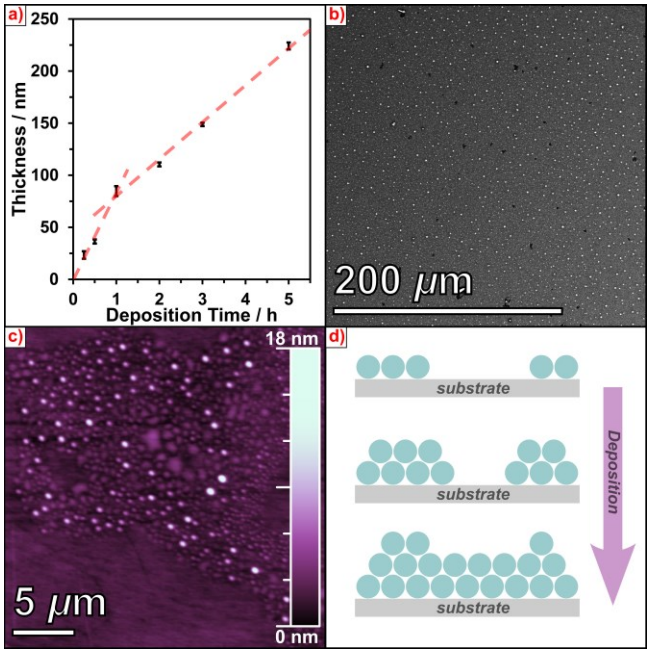

Figure 3: (a) Growth rate for the deposition of MoN_x thin films on soda lime glass substrates by CVD using **1** as a SSP at 400 ºC; film thicknesses were measured using cross-sectional SEM. (b) Plane-view SEM image and (c) AFM image of nanoparticles on a MoN_x film deposited at 400 ºC over 0.5 h. (d) Cartoon representation of the proposed growth mechanism for the MoN_x thin films.

Plane-view SEM analysis of the film deposited for 30 minutes revealed that the substrate was coated with nanoparticles (Figure 3b). The diameter of the particles were determined to be distributed from 0.3 to 2.5 μm (Figure S5), measured by contrast analysis using ImageJ. The size of the particles did not have a gaussian distribution, instead, the number of particles decreased linearly with increasing diameter. This suggests that the diameter of the nanoparticles increase with deposition time. AFM of the

same film showed the particles had a similar size range to that measured by SEM, with a R_{rms} of 14.3 (± 0.6) Å (Figure 3c). In addition, AFM showed that they had an average height of 3.8 nm (Figure S5), however the larger diameter (d = 1.0 μm) particles had heights of 18 nm. The nanoparticles with diameters >1 μm, although observed by SEM, could not be located in the AFM analysis. The nanoparticles that were deposited on the substrate are clearly very flat and wide and are therefore more accurately described as island shaped.

The films deposited with longer deposition times have growth rates in the second regime (2-5 h, Figure 3a). They did not have any nanoparticles or islands at the surface and were instead very smooth (Figures 2c-e). We speculate that the films initially grow by the formation of islands, which eventually coalesce into a continuous MoN_x film (Figure 3d). Once a uniform MoN_x coating has been formed, the deposition likely undergoes Frank-van der Merwe growth,[31] producing the observed featureless films (Figure 2c). Despite having a faster initial growth rate, the films grown with shorter deposition times are not conformal, emphasizing the importance of interrogating the effect of deposition time.

Film Characterization

The elemental composition of the films was determined using X-ray photoelectron spectroscopy (XPS). To avoid oxidation[32,33] *en route* to the XPS facilities, the films were coated with *ca.* 10 nm of Al_2O_3 by atomic layer deposition.[34,35] After sputtering away the Al_2O_3 coating, the Mo 3*d*, N 1*s*, O 1*s*, and C 1*s* core-level spectra were collected. The survey spectra showed a high elemental abundance of Mo (70.0%) and N (24.7%) in the film with minor contributions from other elements (Figure 4e). The high-resolution spectra of Mo 3*d* was deconvoluted into three environments: Mo_2N, MoN/Mo_2N_3, and MoO_2 with the binding energies (BE) of 228.2, 228.8, and 233.1 eV,[36–38] respectively (Figure 4a). In the high-resolution Mo 3*d* spectrum the most significant contribution corresponded to Mo_2N (63.1% by area) indicating that it is the predominate Mo−N type.

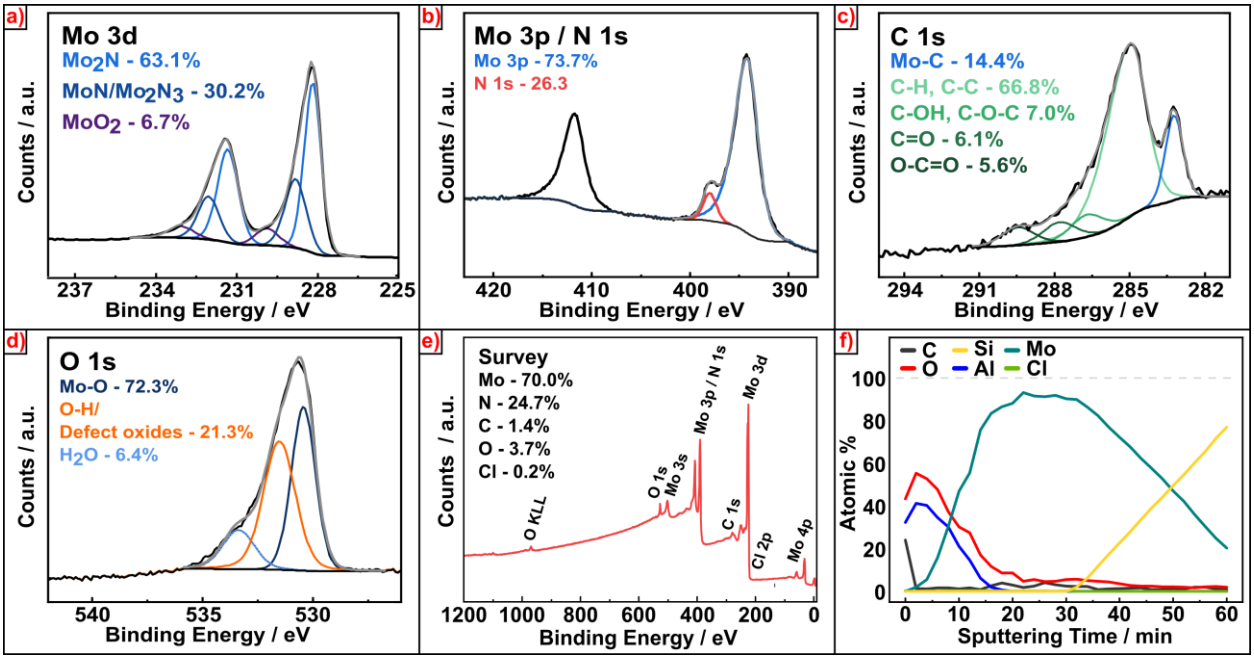

Figure 4: High resolution XPS of a 110 nm MoN_x film deposited at 400 ºC.

The C 1*s* spectrum shows a minor contribution of Mo−C character at 283.3 eV (Figure 4c) from the film, but it is largely composed of signals from the adventitious contaminants C−H/C−C, C−O−C, C=O, and O−C=O with BEs of 285.0, 286.7, 287.8 and 289.5 eV, respectively.[39–41] The film also has slight oxide character but this contribution is quite low as observed in the survey scan. The O 1*s* spectra (Figure 4d) shows that the Mo−O character is located at 530.4 eV, with lattice oxides at 531.5 eV and other low oxygen content arising from the adventitious carbon species.[36,42] The composition of the film is consistent throughout, as shown from sputtering experiments (Figure 4f). However, due to the overlap of the N 1*s* and Mo 3*p* signals, an accurate analysis of N content during sputtering events was not obtained from the survey spectra. The films deposited at 500 ºC and 600 ºC had very similar compositions (Figure S9). The carbon content of MoC_xN_y films prepared by CVD typically increase with increasing deposition temperature, as higher energy decomposition pathways becoming more accessible (*e.g.,* β-CH_3 activation),[14,22] but this was not observed here.

The 110 nm film deposited at 400 ºC was analyzed using grazing-incidence X-ray diffraction (GIXRD). Although the film appeared to be smooth and amorphous by plane-view SEM and AFM (Figures 3d-e), by GIXRD it was found to contain small crystalline

domains. In the broad diffraction pattern (Figure 5), the (111), (200), (220), and (222) reflections originating from the rocksalt form of γ-Mo_2N were clearly observed.[32,43] Additionally, crystalline phases for hexagonal δ-MoN,[10,32] showing the $(20\bar{2}0)$, $(20\bar{2}2)$, and $(22\bar{4}0)$ reflections, were also apparent. The compositions of these observed phases agree with the results from XPS. Additionally, due to the broadness of the diffraction peaks, Mo_3N_2,[44] Mo_2C[45] and MoC[46] phases cannot be ruled out, however because there was minimal carbon in the film, the carbidic phases are not likely present.

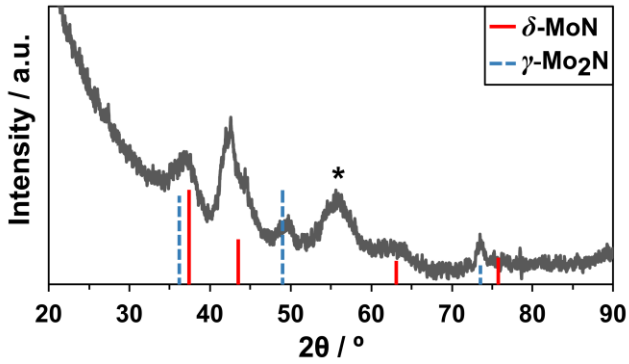

Figure 5: Grazing-incidence (incidence angle of 1º) X-ray diffractogram of a 110 nm MoN_x film deposited at 400 ºC. The reflection at ~55 º is due to the SiO_2/Si(100) substrate.

A proposed mechanism of deposition from **1** to MoN_x is shown in Scheme 1. The incoming precursor **1** likely first loses its dad ligand, which we have previously shown to be labile.[23,29] The $(^tBuN)_2MoCl_2$ surface species can then undergo a γ-H transfer, resulting in the elimination of isobutylene.[23] Finally, the chlorides are likely eliminated as HCl, resulting in the formation of a putative MoN_2 species. MoN_2 is a metastable phase of molybdenum nitride,[47] which can decompose into Mo_2N, MoN, and Mo_3N_2 (Equations 2-4).[21,47,48] Additionally, $Mo_{1-x}N_x$ ($0 \leq x \leq 0.44$) can exhibit multiple phases without a change in enthalpy,[47] with γ-Mo_2N being the most commonly observed phase because of its higher symmetry.[47]

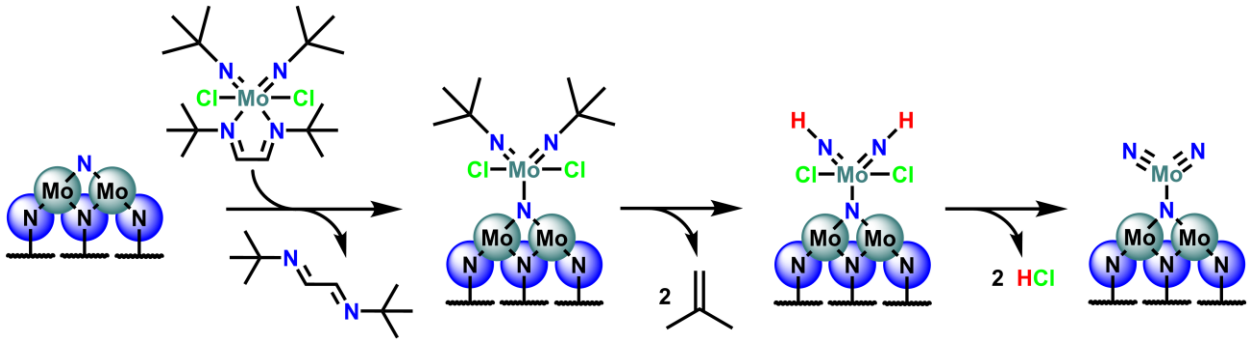

Scheme 1: Proposed mechanism for the CVD of MoN_x using **1** as a SSP. The MoN_2 species likely decomposes primarily into Mo_2N according to Equation 2.

$$4\ MoN_2 \rightarrow\ 2\ Mo_2N + 3\ N_2 \qquad (2)$$

$$2\ MoN_2 \rightarrow\ 2\ MoN + N_2 \qquad (3)$$

$$3\ MoN_2 \rightarrow\ Mo_3N_2 + 2\ N_2 \qquad (4)$$

Conclusions

Here we report the CVD of MoN_x films using $(^tBuN)_2MoCl_2$·dad as a single-source precursor. This process occurs at the lowest temperature used for the single-source CVD of MoN_x films (400 °C). Due to the low temperature of this process, the films are mostly comprised of Mo_2N and MoN, with less than 2% carbon contamination. The films deposited at 400 ºC have a growth rate of 55 nm·h^{-1} and are essentially featureless with a root-mean-square roughness equivalent to that of the underlying substrate. We have previously shown that the dad ligand is labile,[29] and here it was likely able to dissociate from the $(^tBuN)_2MoCl_2$ complex during adsorption. The resulting unligated complex has an uninhibited *γ*-H transfer,[23] therefore decomposition of $(^tBuN)_2MoCl_2$ proceeds with a relatively low barrier, outcompeting the higher energy *β*-CH_3 decomposition pathway and preventing incorporation of carbon into the film. Thus, pure MoN_x films were prepared, guided by our previous investigations into the mechanism of precursor decomposition.

Experimental Section

General Experimental. All manipulations were performed under air-free conditions using either standard Schlenk techniques or in a nitrogen-filled (99.998% purity) MBraun

glovebox. (^{t}BuN)$_2$MoCl$_2$·dme,[49,50] and 1,4-di-*tert*-butyl-1,3-diazabutadiene (dad)[51] were prepared following known methods. All solvents (ACS reagent-grade) were purified using an MBraun Solvent Purification System and were stored over 4 Å molecular sieves. All glassware was oven-dried at 130 ºC, for at least 3 h, prior to use. ^{1}H NMR spectra were collected on a Bruker AVANCE 300 MHz spectrometer, at room temperature.

Synthesis of (^{t}BuN)$_2$MoCl$_2$·dad (1). The precursor was prepared following a known method.[29] 1,4-Di-*tert*-butyl-1,3-diazabutadiene (5.837 g, 34.68 mmol) was added to a solution of the (^{t}BuN)$_2$MoCl$_2$·dme (12.250 g, 30.68 mmol) in 100 mL of THF. The mixture was stirred at room temperature for 8 hours then the volatiles were removed under reduced pressure resulting in a yellow solid. The material was suspended in 30 mL of pentane and the resultant mixture was stirred vigorously for 20 minutes. The solids were then collected on a sintered glass frit and were washed with three, 10 mL portions of diethyl ether. The resulting pale-yellow powder was then recrystallized from 40 mL of dichloromethane, layered with 10 mL of pentane. After 24 hours at −30 ºC yellow/orange crystals were isolated by decanting the mother-liquor; these were subsequently dried *in vacuo* and ground, in a mortar, into a yellow powder. Yield = 13.481 g (28.24 mmol, 92%). ^{1}H NMR (300 MHz, C_6D_6, ppm): δ 1.45 (s, 18H, C(C*H*$_3$)$_3$), 1.57 (s, 18H, Mo=NC(C*H*$_3$)$_3$), 7.36 (s, 2H, N=C*H*).

Thermolysis of 1. A piece of a glass microscope slide (*ca.* 1 x 1 cm^2) and **1** (0.202 g, 0.423 mmol) were loaded into a 50 mL Schlenk tube and which was then placed under static vacuum (40 mTorr). The Schlenk tube was thoroughly heated with a heat gun to ensure the entire flask was hot, to prevent condensation of the precursor. The Schlenk tube was then thoroughly heated with a propane torch which resulted in the immediate formation of a mirror-like film inside the entirety of the tube. After thermolysis, the glass substrate was removed from the tube and was analyzed by EDS.

Thin Film Deposition. CVD of MoN_x was performed in a home-built, horizontal flow, low-pressure, hot-walled reactor that we described previously.[52,53] The precursor **1** was ground into a fine powder with a pestle and mortar to try to ensure a constant surface

area. **1** was loaded, under air-free conditions, into a 10 mL beaker with an inner diameter of 25 mm, which was placed inside of a stainless-steel, pass-through bubbler. The reactor was loaded with four untreated soda lime glass microscope slides (Globe Scientific), aligned linearly in the direction of flow. A piece of a silicon (100) wafer (with native oxide) was also placed on top of the glass slide that was in the center of the deposition chamber. The deposition chamber (base pressure of 70 mTorr) was heated to the specified temperature for 1 h prior to the deposition experiments to ensure constant temperature. The bubbler holding **1** was heated to 105 ºC with nitrogen (50 sccm, 99.998%) as a carrier gas, which resulted in a typical delivery of ~1 $mg \cdot min^{-1}$; the bubbler was also held at 105 ºC for 1 h prior to the deposition to ensure constant temperature. The precursor delivery lines connecting the bubbler to the deposition chamber were heated to 120 ºC to prevent condensation. During the deposition experiments the valves of the bubbler were opened to allow the delivery of **1** into the reaction chamber. After the deposition, the valves to the precursor bubbler were closed and the deposition chamber was left at the deposition temperature for 1 h, still under a flow of nitrogen. It was then cooled to 200 ºC, at which point the substrates were unloaded into air.

Al_2O_3 Coating. The MoN_x thin films appeared to be susceptible to oxidation, therefore one film was coated with Al_2O_3 to protect it from oxidation prior to compositional analysis. Following the general deposition procedure outlined above a 110 nm MoN_x film was prepared from a 2 h deposition at 400 ºC. After the deposition, the chamber was cooled to 100 ºC, under a constant flow of nitrogen. The film was then coated with ~ 10 nm of Al_2O_3 by atomic layer deposition using trimethylaluminum (TMA) and H_2O.[54] The pulse sequence was TMA: 0.1 s | N_2 purge: 15 s | H_2O: 0.1 s | N_2 purge: 15 s, and 100 cycles were performed. After the deposition the Si and glass substrates were unloaded into air and were quickly transferred to a glovebox and were stored under nitrogen until they were analyzed.

Thin Film Analysis. Scanning electron microscopy was performed on samples with an accelerating voltage of 20 kV using a Tescan Vega-II XMU SEM in both secondary electron and backscatter electron imaging modes. MoN_x films on glass were coated with

<10 nm of gold using a Quorum Q150T ES sputter/evaporator (45 s, 20 mA, 10^{-3} mbar) prior to analysis by SEM to ensure continuous conductivity. The size distribution of nanoparticles was determine using ImageJ.[55] Energy dispersive X-ray spectroscopy was obtained with an Oxford Inca Energy 250X EDS using a working distance of 10 nm. Atomic force microscopy measurements were performed on a Bruker Dimension Edge 3100 SPM/AFM instrument and data analysis was conducted using WSxM 5.0.[56] Step edges for AFM were obtained by scratching the surface of the MoN_x films with a diamond-tipped scribe. X-ray diffraction measurements were collected using grazing-incidence (incidence angle of 1º) and were collected on a Malvern PANalytical Empyrean X-ray diffractometer using Cu K*α* radiation. UV/Vis measurements were performed using an Agilent Technologies Cary 5000 spectrophotometer.

X-Ray Photoelectron Spectroscopy. XPS analyses were carried out at Surface Science Western (SSW) with a Kratos AXIS Supra X-ray photoelectron spectrometer using a monochromatic Al Kα source (15 mA, 15 kV). The sample has a depth of 7−10 nm and has detection limits ranging from 0.1 to 0.5 atomic percent. The instrument work function was calibrated to give a BE of 285 eV for the C 1s spectrum. The Kratos charge neutralizer system was used on all specimens. Both the survey scan and high-resolution analyses were collected at a takeoff angle of 90° with an analysis area of 300 × 700 *μ*m, and a pass energy of 15 eV. CasaXPS (ver. 2.3.23) software was used for all deconvolution of spectra with a Shirley background subtraction. Spectral interpretation and fittings were done with fitting parameters and constraints collected from NIST. Depth profile experiments used an Ar cluster gun with 5 keV accelerating voltage and 500 Ar atoms with 120 second intervals between survey spectra. and then modelled using Gaussian−Lorentzian functions and Sherley background subtraction. A custom peak shape (LA 2.6, 4, 7) was modelled from the Mo $3p_{1/2}$ signal at 411.7 eV in the Mo 3*p* high-resolution spectrum and applied to the identically shaped Mo $3p_{3/2}$ signal. This allowed for the appropriate fitting of the N 1*s* signal and determination of the overall nitrogen content. From this deconvolution method, a ratio of 73.7:26.3, Mo:N was determined which allowed for the identification of the other elemental contributions.

Supporting Information

QCM data, SEM and AFM images, EDS spectra, UV-Vis spectra, and GIXRD results can be found in the SI.

Author Information

Corresponding Author

*E-mail: Michael.land@carleton.ca

ORCID

Michael A. Land: 0000-0001-5861-242X

Justin T. Lomax: 0000-0002-6034-2163

Seán T. Barry: 0000-0001-5515-4734

Author Contributions

The manuscript was written through contributions of all authors. All authors have given approval to the final version of the manuscript.

Acknowledgements

M.A.L. thanks the Natural Sciences and Engineering Council of Canada (NSERC) for funding through the Alexander Graham Bell CGS-D Scholarship. J.T.L thanks the Ontario Graduate Scholarship (OGS) Program and Surface Science Western (SSW; Drs. M. Biesinger and J. Henderson) for their support. S.T.B. acknowledges NSERC for support through the Discovery Grants Program (RGPIN-2019-06213). Finally, we also thank Eden Goodwin for technical assistance, Dr. Jianqun Wang for SEM assistance, Dr. Peter Gordon for AFM acquisition, and Dr. Peter Pallister for GIXRD acquisition.

References

(1) Alén, P.; Ritala, M.; Arstila, K.; Keinonen, J.; Leskelä, M. Atomic Layer Deposition of Molybdenum Nitride Thin Films for Cu Metallizations. *J. Electrochem. Soc.* **2005**, *152*, G361.

(2) Jang, Y.; Kim, J. B.; Hong, T. E.; Yeo, S. J.; Lee, S.; Jung, E. A.; Park, B. K.; Chung, T.-M.; Kim, C. G.; Lee, D.-J.; Lee, H.-B.-R.; Kim, S.-H. Highly-Conformal Nanocrystalline Molybdenum Nitride Thin Films by Atomic Layer Deposition as a Diffusion Barrier against Cu. *J. Alloys Compd.* **2016**, *663*, 651–658.

(3) Valli, J.; Mäkelä, U.; Hentzell, H. T. G. Tribological Properties of MoN x Coatings in Contact with Copper. *J. Vac. Sci. Technol. A,* **1986**, *4*, 2850–2854.

(4) Zhu, X.; Yue, D.; Shang, C.; Fan, M.; Hou, B. Phase Composition and Tribological Performance of Molybdenum Nitride Coatings Synthesized by IBAD. *Surf. Coat. Technol.* **2013**, *228*, S184–S189.

(5) Lévy, F.; Hones, P.; Schmid, P. E.; Sanjinés, R.; Diserens, M.; Wiemer, C. Electronic States and Mechanical Properties in Transition Metal Nitrides. *Surf. Coat. Technol.* **1999**, *120–121*, 284–290.

(6) Nandi, D. K.; Sen, U. K.; Choudhury, D.; Mitra, S.; Sarkar, S. K. Atomic Layer Deposited Molybdenum Nitride Thin Film: A Promising Anode Material for Li Ion Batteries. *ACS Appl. Mater. Interfaces,* **2014**, *6*, 6606–6615.

(7) Liu, J.; Tang, S.; Lu, Y.; Cai, G.; Liang, S.; Wang, W.; Chen, X. Synthesis of Mo2N Nanolayer Coated MoO_2 Hollow Nanostructures as High-Performance Anode Materials for Lithium-Ion Batteries. *Energy Environ. Sci.* **2013**, *6*, 2691–2697.

(8) Ramesh, R.; Nandi, D. K.; Kim, T. H.; Cheon, T.; Oh, J.; Kim, S. H. Atomic-Layer-Deposited MoN_x Thin Films on Three-Dimensional Ni Foam as Efficient Catalysts for the Electrochemical Hydrogen Evolution Reaction. *ACS Appl. Mater. Interfaces,* **2019**, *11*, 17321–17332.

(9) Mohimi, E.; Canova, K.; Zhang, Z.; Liu, S.; Mallek, J. L.; Girolami, G. S.; Abelson, J. R. Low Temperature Chemical Vapor Deposition of Superconducting Molybdenum Carbonitride Thin Films. *J. Vac. Sci. Technol. A,* **2019**, *37*, 021503.

(10) Ganin, A. Y.; Kienle, L.; Vajenine, G. V. Synthesis and Characterisation of Hexagonal Molybdenum Nitrides. *J. Solid State Chem.* **2006**, *179*, 2339–2348.

(11) Sun, S.-C.; Chiu, H.-T. MOCVD Molybdenum Nitride Diffusion Barrier for Cu Metallization. US6114242A, 2000.

(12) Miikkulainen, V.; Suvanto, M.; Pakkanen, T. A. Atomic Layer Deposition of Molybdenum Nitride from Bis(Tert-Butylimido)- Bis(Dimethylamido)Molybdenum and Ammonia onto Several Types of Substrate Materials with Equal Growth per Cycle. *Chem. Mater.* **2007**, *19*, 263–269.

(13) Cho, Y. K.; Choi, Y.; Kim, S.-G.; Jun, Y.; Kim, H. Influence of Hydrogen Supply on Mo(C,N) Films Synthesized by Plasma-Enhanced Chemical Vapor Deposition

Using Bis(Tert-butylimido) Bis(Dimethylamido) Molybdenum. *Thin Solid Films,* **2019**, *692*, 137607.

(14) Chiu, H. T.; Ho, W. Y.; Chuang, S. H. Deposition of Molybdenum Carbonitride Thin Films from $Mo(NBut)_2(NHBut)_2$. *J. Mater. Res.* **1994**, *9*, 1622–1624.

(15) Ou, N. C.; Preradovic, K.; Ferenczy, E. T.; Sparrow, C. B.; Germaine, I. M.; Jurca, T.; Craciun, V.; Mcelwee-White, L. Synthesis and Evaluation of Molybdenum Imido-Thiolato Complexes for the Aerosol-Assisted Chemical Vapor Deposition of Nitrogen-Doped Molybdenum Disulfide. *Organometallics,* **2020**, *39*, 956–966.

(16) Gwildies, V.; Thiede, T. B.; Amirjalayer, S.; Alsamman, L.; Devi, A.; Fischer, R. A. All-Nitrogen Coordinated Amidinato/Imido Complexes of Molybdenum and Tungsten: Syntheses and Characterization. *Inorg. Chem.* **2010**, *49*, 8487–8494.

(17) Thiede, T.; Gwildies, V.; Alsamann, L.; Rische, D.; Fischer, R. Novel Precursors for the MOCVD of Molybdenum Nitride. *ECS Trans.* **2009**, *25*, 593–600.

(18) Srinivasan, N. B.; Thiede, T. B.; de los Arcos, T.; Gwildies, V.; Krasnopolski, M.; Becker, H. W.; Rogalla, D.; Devi, A.; Fischer, R. A. Transition Metal Nitride Thin Films Grown by MOCVD Using Amidinato Based Complexes $[M(NtBu)_2\{(IPrN)_2CMe\}_2]$ (M=Mo, W) as Precursors. *Surf. Coat. Technol.* **2013**, *230*, 130–136.

(19) Rische, D. MOCVD of Tungsten and Molybdenum Nitrides, Ph.D. Thesis, University of Bochum, Bochum, Germany, 2007.

(20) Land, M. A.; Dimova, D. A.; Robertson, K. N.; Barry, S. T. Cut-and-Pasting Ligands: The Structure/Function Relationships of a Thermally Robust Mo(VI) Precursor. *J. Vac. Sci. Technol. A,* **2023**, *41*, 012403.

(21) Dezelah IV, C. L.; El-Kadri, O. M.; Heeg, M. J.; Winter, C. H. Preparation and Characterization of Molybdenum and Tungsten Nitride Nanoparticles Obtained by Thermolysis of Molecular Precursors. *J. Mater. Chem.* **2004**, *14*, 3167–3176.

(22) Chiu, H.-T.; Chang, G.-B.; Ho, W.-Y.; Chuang, S.-H.; Lee, G.-H.; Peng, S.-M. Syntheses and X-Ray Crystal Structures of Dichlorobis(Tert-Butylimido) Complexes of Molybdenum(VI); Potential Precursors to Molybdenum Nitride and Molybdenum Carbonitride. *J. Chin. Chem. Soc.* **1994**, *41*, 755–761.

(23) Land, M. A.; Bačić, G.; Robertson, K. N.; Barry, S. T. Origin of Decomposition in a Family of Molybdenum Precursor Compounds. *Inorg. Chem.* **2022**, *61*, 16607–16621.

(24) Blakeney, K. J.; Winter, C. H. Thermal Atomic Layer Deposition of Tungsten Carbide Films from WCl_6 and $AlMe_3$. *J. Vac. Sci. Technol. A,* **2018**, *36*, 01A104.

(25) Wu, J.; Li, J.; Zhou, C.; Lei, X.; Gaffney, T.; Norman, J. A. T.; Li, Z.; Gordon, R.; Cheng, H. Computational Study on the Relative Reactivities of Cobalt and Nickel Amidinates via β-H Migration. *Organometallics,* **2007**, *26*, 2803–2805.

(26) Miikkulainen, V.; Suvanto, M.; Pakkanen, T. A. Bis(Tert-Butylimido)-Bis(Dialkylamido) Complexes of Molybdenum as Atomic Layer Deposition (ALD) Precursors for Molybdenum Nitride: The Effect of the Alkyl Group. *Chem. Vap. Deposition,* **2008**, *14*, 71–77.

(27) Volpe, L.; Boudart, M. Compounds of Molybdenum and Tungsten with High Specific Surface Area. *J. Solid State Chem.* **1985**, *59*, 348–356.

(28) Land, M. A.; Robertson, K. N.; Barry, S. T. Ligand-Assisted Volatilization and Thermal Stability of Bis(Imido)Dichloromolybdenum(VI) ([(t-BuN═)$_2$MoCl$_2$]$_2$) and Its Adducts. *Organometallics,* **2020**, *39*, 916–927.

(29) Land, M. A.; Bačić, G.; Robertson, K. N.; Barry, S. T. Thermal Stability and Decomposition Pathways in Volatile Molybdenum(VI) Bis-Imides. *Inorg. Chem.* **2022**, *61*, 4980–4994.

(30) Tsai, M. H.; Sun, S. C.; Chiu, H. T.; Chuang, S. H. Metalorganic Chemical Vapor Deposition of Tungsten Nitride for Advanced Metallization. *Appl. Phys. Lett.* **1996**, *68*, 1412–1414.

(31) Bauer, E. Phänomenologische Theorie Der Kristallabscheidung an Oberflächen. I. *Z. Kristallogr. Cryst. Mater.* **1958**, *110*, 395–431.

(32) Kreider, M. E.; Stevens, M. B.; Liu, Y.; Patel, A. M.; Statt, M. J.; Gibbons, B. M.; Gallo, A.; Ben-Naim, M.; Mehta, A.; Davis, R. C.; Ievlev, A. V.; Nørskov, J. K.; Sinclair, R.; King, L. A.; Jaramillo, T. F. Nitride or Oxynitride? Elucidating the Composition–Activity Relationships in Molybdenum Nitride Electrocatalysts for the Oxygen Reduction Reaction. *Chem. Mater.* **2020**, *32*, 2946–2960.

(33) Solak, N.; Ustel, F.; Urgen, M.; Aydin, S.; Cakir, A. F. Oxidation Behavior of Molybdenum Nitride Coatings. *Surf. Coat. Technol.* **2003**, *174–175*, 713–719.

(34) Paussa, L.; Guzman, L.; Marin, E.; Isomaki, N.; Fedrizzi, L. Protection of Silver Surfaces Against Tarnishing by Means of Alumina/Titania-Nanolayers. *Surf. Coat. Technol.* **2011**, *206* (5), 976–980.

(35) Díaz, B.; Härkönen, E.; Światowska, J.; Maurice, V.; Seyeux, A.; Marcus, P.; Ritala, M. Low-Temperature Atomic Layer Deposition of Al_2O_3 Thin Coatings for Corrosion Protection of Steel: Surface and Electrochemical Analysis. *Corros. Sci.* **2011**, *53*, 2168–2175.

(36) Spevack, P. A.; McIntyre, N. S. Thermal Reduction of MoO_3. *J. Phys. Chem.* **1992**, *96*, 9029–9035.

(37) Quincy, R. B.; Houalla, M.; Proctor, A.; Hercules, D. M. Distribution of Molybdenum Oxidation States in Reduced Mo/TiO_2 Catalysts: Correlation with Benzene Hydrogenation Activity. *J. Phys. Chem.* **1990**, *94*, 1520–1526.

(38) Choi, J. G.; Brenner, J. R.; Colling, C. W.; Demczyk, B. G.; Dunning, J. L.; Thompson, L. T. Synthesis and Characterization of Molybdenum Nitride Hydrodenitrogenation Catalysts. *Catal. Today* **1992**, *15*, 201–222.

(39) Biesinger, M. C. Accessing the Robustness of Adventitious Carbon for Charge Referencing (Correction) Purposes in XPS Analysis: Insights from a Multi-User Facility Data Review. *Appl. Surf. Sci.* **2022**, *597*, 153681.

(40) Wang, J.; Castonguay, M.; Deng, J.; McBreen, P. H. RAIRS and TPD Study of CO and NO on β-Mo_2C. *Surf. Sci.* **1997**, *374*, 197–207.

(41) St. Clair, T. P.; Oyama, S. T.; Cox, D. F.; Otani, S.; Ishizawa, Y.; Lo, R.-L.; Fukui, K.; Iwasawa, Y. Surface Characterization of α-Mo_2C (0001). *Surf. Sci.* **1999**, *426*, 187–198.

(42) Schroeder, T.; Zegenhagen, J.; Magg, N.; Immaraporn, B.; Freund, H. J. Formation of a Faceted MoO_2 Epilayer on Mo(112) Studied by XPS, UPS and STM. *Surf. Sci.* **2004**, *552*, 85–97.

(43) Bull, C. L.; Kawashima, T.; McMillan, P. F.; Machon, D.; Shebanova, O.; Daisenberger, D.; Soignard, E.; Takayama-Muromachi, E.; Chapon, L. C. Crystal Structure and High-Pressure Properties of γ-Mo_2N Determined by Neutron Powder Diffraction and X-Ray Diffraction. *J. Solid State Chem.* **2006**, *179*, 1762–1767.

(44) Lee, K.-H.; Lee, Y.-W.; Ko, A.-R.; Cao, G.; Park, K.-W. Single-Crystalline Mesoporous Molybdenum Nitride Nanowires with Improved Electrochemical Properties. *J. Am. Ceram. Soc.* **2013**, *96*, 37–39.

(45) Ge, Y.; Song, H.; Bao, K.; Ma, S.; Li, L.; Tao, Q.; Zhu, P.; Liu, B.; Duan, D.; Cui, T. A Novel Hard Superconductor Obtained in Di-Molybdenum Carbide (Mo_2C) with Mo–C Octahedral Structure. *J. Alloys Compd.* **2021**, *881*, 160631.

(46) Schuster, J.; Rudy, E.; Nowotny, H. The “MoC”-Phase with WC Structure. *Monatsh. Chem.* **1976**, *107*, 1167–1176.

(47) Balasubramanian, K.; Huang, L.; Gall, D. Phase Stability and Mechanical Properties of Mo 1- x N x with 0 ≤ x ≤ 1. *J. Appl. Phys.* **2017**, *122*, 195101.

(48) Wang, S.; Ge, H.; Sun, S.; Zhang, J.; Liu, F.; Wen, X.; Yu, X.; Wang, L.; Zhang, Y.; Xu, H.; Neuefeind, J. C.; Qin, Z.; Chen, C.; Jin, C.; Li, Y.; He, D.; Zhao, Y. A New Molybdenum Nitride Catalyst with Rhombohedral MoS_2 Structure for Hydrogenation Applications. *J. Am. Chem. Soc.* **2015**, *137*, 4815–4822.

(49) Fox, H. H.; Yap, K. B.; Robbins, J.; Cai, S.; Schrock, R. R. Simple-High Yield Syntheses of Molybdenum(VI) Bis(IMIDO) Complexes of the Type $Mo(NR)_2Cl_2$(1,2-Dimethoxyethane). *Inorg. Chem.* **1992**, *31*, 2287–2289.

(50) Dyer, P. W.; Gibson, V. C.; Howard, J. A. K.; Whittle, B.; Wilson, C. Four Coordinate Bis(Imido) Alkene Complexes of Molybdenum(IV): Relatives of the Zirconocene Family. *J. Chem. Soc., Chem. Commun.* **1992**, *04*, 1666–1668.

(51) Kim, S. B.; Sinsermsuksakul, P.; Hock, A. S.; Pike, R. D.; Gordon, R. G. Synthesis of N-Heterocyclic Stannylene (Sn(II)) and Germylene (Ge(II)) and a Sn(II) Amidinate and Their Application as Precursors for Atomic Layer Deposition. *Chem. Mater.* **2014**, *26*, 3065–3073.

(52) Zhou, W.; Mandia, D. J.; Griffiths, M. B. E.; Bialiayeu, A.; Zhang, Y.; Gordon, P. G.; Barry, S. T.; Albert, J. Polarization-Dependent Properties of the Cladding Modes of a Single Mode Fiber Covered with Gold Nanoparticles. *Opt. Express* **2013**, *21*, 245.

(53) Zanders, D.; Bačić, G.; Leckie, D.; Odegbesan, O.; Rawson, J.; Masuda, J. D.; Devi, A.; Barry, S. T. A Rare Low-Spin Co IV Bis(B-silyldiamide) with High Thermal Stability: Steric Enforcement of a Doublet Configuration. *Angew. Chem. Int. Ed.* **2020**, *59*, 14138–14142.

(54) Puurunen, R. L. Surface Chemistry of Atomic Layer Deposition: A Case Study for the Trimethylaluminum/Water Process. *J. Appl. Phys.* **2005**, *97*, 121301.

(55) Schneider, C. A.; Rasband, W. S.; Eliceiri, K. W. NIH Image to ImageJ: 25 Years of Image Analysis. *Nat. Methods,* **2012**, *9*, 671–675.

(56) Horcas, I.; Fernández, R.; Gómez-Rodríguez, J. M.; Colchero, J.; Gómez-Herrero, J.; Baro, A. M. WSXM: A Software for Scanning Probe Microscopy and a Tool for Nanotechnology. *Rev. Sci. Instrum.* **2007**, *78*, 013705.